


# Dimeric assembly of human Suv3 helicase promotes its RNA unwinding function in mitochondrial RNA degradosome for RNA decay

Monika Jain<sup>1,2</sup> | Bagher Golzarroshan<sup>2</sup> | Chia-Liang Lin<sup>2</sup> | Sashank Agrawal<sup>2</sup> | Wei-Hsuan Tang<sup>2,3</sup> | Chiu-Ju Wu<sup>2,3</sup> | Hanna S. Yuan<sup>1,2,3</sup> 

<sup>1</sup>Molecular and Cell Biology, Taiwan International Graduate Program, Academia Sinica and Graduate Institute of Life Sciences, National Defense Medical Center, Taipei, Taiwan

<sup>2</sup>Institute of Molecular Biology, Academia Sinica, Taipei, Taiwan

<sup>3</sup>Graduate Institute of Biochemistry and Molecular Biology, National Taiwan University, Taipei, Taiwan

## Correspondence

Hanna S. Yuan, Institute of Molecular Biology, Academia Sinica, Taipei 11529, Taiwan.

Email: [hanna@sinica.edu.tw](mailto:hanna@sinica.edu.tw)

Website: <http://hyuan.imb.sinica.edu.tw>

## Funding information

Academia Sinica, Taiwan, Grant/Award Number: AS-IA-110-L02

**Review editor:** John Kuriyan

## Abstract

Human Suv3 is a unique homodimeric helicase that constitutes the major component of the mitochondrial degradosome to work cooperatively with exoribonuclease PNPase for efficient RNA decay. However, the molecular mechanism of how Suv3 is assembled into a homodimer to unwind RNA remains elusive. Here, we show that dimeric Suv3 preferentially binds to and unwinds DNA–DNA, DNA–RNA, and RNA–RNA duplexes with a long 3′ overhang ( $\geq 10$  nucleotides). The C-terminal tail (CTT)-truncated Suv3 (Suv3 $\Delta$ C) becomes a monomeric protein that binds to and unwinds duplex substrates with  $\sim$ six to sevenfold lower activities relative to dimeric Suv3. Only dimeric Suv3, but not monomeric Suv3 $\Delta$ C, binds RNA independently of ATP or ADP, and is capable of interacting with PNPase, indicating that dimeric Suv3 assembly ensures its continuous association with RNA and PNPase during ATP hydrolysis cycles for efficient RNA degradation. We further determined the crystal structure of the apo-form of Suv3 $\Delta$ C, and SAXS structures of dimeric Suv3 and PNPase–Suv3 complex, showing that dimeric Suv3 caps on the top of PNPase via interactions with S1 domains, and forms a dumbbell-shaped degradosome complex with PNPase. Overall, this study reveals that Suv3 is assembled into a dimeric helicase by its CTT for efficient and persistent RNA binding and unwinding to facilitate interactions with PNPase, promote RNA degradation, and maintain mitochondrial genome integrity and homeostasis.

## KEYWORDS

mitochondrial homeostasis, mitochondrial RNA degradation, RNA helicase, RNA metabolism, RNA turnover

## 1 | INTRODUCTION

Suv3 is an ATP-dependent RNA–DNA helicase first discovered in yeast as a suppressor of yal1 deletion

phenotype.<sup>1</sup> Subsequently, the human homolog was identified, showing that Suv3 is a highly conserved protein expressed in all eukaryotic species.<sup>2</sup> Sequence analysis further revealed that Suv3 is a superfamily 2 (SF2) helicase

This is an open access article under the terms of the [Creative Commons Attribution-NonCommercial-NoDerivs](https://creativecommons.org/licenses/by-nc-nd/4.0/) License, which permits use and distribution in any medium, provided the original work is properly cited, the use is non-commercial and no modifications or adaptations are made.

© 2022 The Authors. *Protein Science* published by Wiley Periodicals LLC on behalf of The Protein Society.

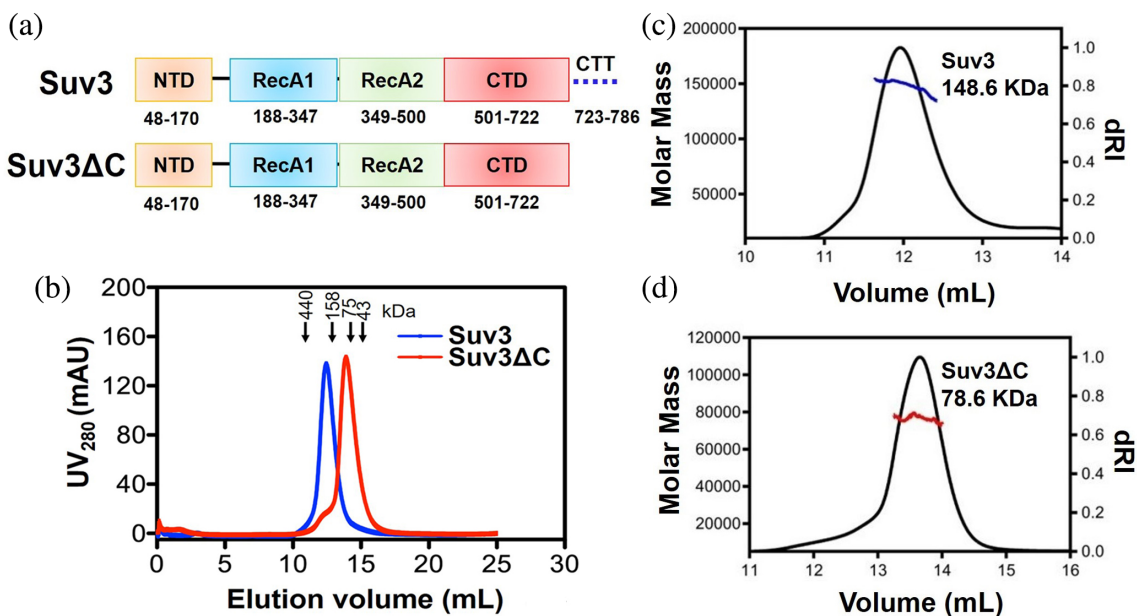


**FIGURE 1** Human Suv3 is a dimeric protein and CTT-truncated Suv3 (Suv3 $\Delta$ C) is monomeric. (a) Domain organization of full-length Suv3 (48–786 residues) and C-terminal tail (CTT)-truncated Suv3 $\Delta$ C (48–722 residues). (b) Elution profiles of Suv3 (blue) and Suv3 $\Delta$ C (red) in the gel filtration chromatographic column (Superdex 200 10/300 GL), revealing that Suv3 eluted as a homodimer whereas Suv3 $\Delta$ C eluted as a monomer. Protein markers: Ferritin (440 kDa), aldolase (158 kDa), conalbumin (75 kDa), and ovalbumin (43 kDa). (C–D) The molecular weights of Suv3 of 148.6 kDa (calculated MW of Suv3 dimer with a His-tag: 170 kDa), and Suv3 $\Delta$ C of 78.6 kDa (calculated MW of Suv3 $\Delta$ C monomer with a His-tag: 85.3 kDa) were determined by size exclusion chromatography-coupled multi-angle light scattering (SEC-MALS)

containing two typical RecA-like domains (RecA1 and RecA2) that constitute its helicase core.<sup>3,4</sup> Suv3 was previously classified in the sub-group of Ski2-like DEXH RNA helicases in SF2, however, due to the structure dissimilarity and significant differences in the key residues of DEIQ, but not DEXH, in the motif II, Suv3 is suggested to be separately grouped.<sup>5,6</sup> Besides the two RecA-like domains, Suv3 also contains three auxiliary domains, that is, an N-terminal domain (NTD), a C-terminal domain (CTD) and a C-terminal tail (CTT), as well as a mitochondrial localization signal in its N-terminal end (Figure 1A).<sup>7</sup> Human Suv3 is thus a unique SF2 helicase predominantly localized in the mitochondrial matrix where it plays important roles in maintaining mitochondrial homeostasis.<sup>8</sup>

Suv3 is a multi-substrate helicase and unwinds double-stranded RNA, DNA, and DNA–RNA heteroduplex.<sup>9</sup> The most extensively characterized biological function of Suv3 in mitochondria is unwinding of RNA duplex as part of RNA surveillance and degradation pathways.<sup>10</sup> Suv3 interacts with a 3′–5′ exoribonuclease to form the RNA-degrading machinery, termed the mitochondrial degradosome, in mitochondrial granules (foci) that can degrade structured RNA with a 3′ overhang from the 3′ to 5′ end in an ATP-dependent manner.<sup>11,12</sup> Yeast Suv3 interacts with the exoribonuclease Dss1 to form a 1-to-1 complex,<sup>13,14</sup> whereas human Suv3 interacts with the exoribonuclease PNPase to form the 2-to-3 complex

of the mitochondrial degradosome.<sup>11,12,15</sup> Loss of Suv3 in yeast,<sup>16</sup> Drosophila,<sup>17</sup> or mice<sup>18</sup> results in an accumulation of mitochondrial mRNAs, mitochondrial dysfunction, and lethal phenotypes. Reduced Suv3 expression in human cell lines and heterozygous knockout of Suv3 in mice both caused genome instability, manifesting as an increased population of mutations in mitochondrial DNA (mtDNA) and decreased mtDNA copy number, leading to tumor development and shortened lifespan.<sup>19</sup> The accumulated double-stranded RNA (dsRNA) resulting from loss of PNPase or Suv3 can escape into the cytoplasm, where it engages antiviral signaling pathways to trigger a type I interferon response.<sup>20,21</sup> Therefore, Suv3 prevents activation of potent innate immune defense mechanisms stimulated by mitochondrial dsRNA.

Apart from RNA degradation, Suv3 is also involved in unwinding RNA–DNA hybrid duplexes to prevent harmful formation of R-loops during transcription in mitochondria.<sup>22</sup> These stable R-loops can block the replication and transcription machineries, leading to mitochondrial genome instability and disease. Moreover, a small proportion of Suv3 is located in the nucleus, consistent with the observation that the protein harbors a nuclear localization sequence (NLS) at its C-terminal end.<sup>23</sup> In the nucleus, Suv3 interacts with WRN and BLM helicases, FEN1 flap endonuclease, as well as replication protein A, which are involved in DNA recombination,

repair and/or replication.<sup>18,24</sup> Therefore, not only is Suv3 a key player in regulating mitochondrial genome stability and mitochondrial homeostasis, but it may also have multiple roles in nuclear DNA metabolism.

The crystal structure of a truncated form of human Suv3 (residues 47–722) in complex with a five-nucleotide RNA (PDB entry: 3RC8) has been reported previously, revealing that it is a monomer and its RecA1 and RecA2 domains together with CTD make a ring-like structure to bind RNA.<sup>6</sup> However, a dimeric Suv3, but not a monomeric one, interacts with trimeric PNPase to form a 2-to-3 assembly of mitochondrial degradosome. A similar 2-to-3 assembly of a dimeric DEAD-box helicase in complex with a trimeric PNPase has also been documented in bacterial RNA degradosome, with Gram-negative *Escherichia coli* RhlB helicase forming a complex with PNPase, and Gram-positive *Bacillus subtilis* CshA helicase forming a complex with PNPase.<sup>25–28</sup> The crystal structure of CshA from *Geobacillus stearothermophilus* reveals a V-shaped dimeric structure, with the two helicase core domains located in two arms that are linked by C-terminal dimerization domains.<sup>29</sup> Apart from the homologous RecA-like domains in the helicase core, Suv3 does not share any similar auxiliary domains with CshA, nor does it contain a dimerization domain similar to those found in certain dimeric DEAD-box helicases, including Hera, CsdA, DDX50, and DDX21.<sup>30</sup> Accordingly, we were intrigued as to how human Suv3 is assembled into a homodimer and why it functions as a dimeric helicase for RNA unwinding in the mitochondrial degradosome.

Here, we have investigated the biochemical and enzymatic properties of Suv3 in terms of its RNA binding and unwinding abilities. We show that the C-terminal tail (CTT) of Suv3 (amino acids 723–786) is required for dimerization and efficient RNA unwinding activity and, moreover, that dimeric assembly of Suv3 ensures continuous RNA substrate association and interactions with PNPase during ATP hydrolysis cycles. We further determined the crystal structure of the apo-form of a monomeric Suv3 and revealed the molecular models of Suv3 helicase and Suv3–PNPase complex via small-angle X-ray scattering (SAXS) analyses. Our study illustrates that Suv3 has to assemble into a homodimer for efficient and persistent RNA binding and unwinding, as well as interactions with PNPase, enabling it to exert its roles in RNA decay.

## 2 | RESULTS

### 2.1 | Suv3 forms a homodimer via its C-terminal tail

To examine the molecular assembly of Suv3, we generated two constructs to express N-terminal His-tagged

Suv3 (residues 48–786) and CTT-truncated Suv3 (Suv3 $\Delta$ C, residues 48–722), both of which lacked the mitochondrial targeting sequence (residues 1–47) (Figure 1A). The recombinant proteins were expressed in *E. coli* and purified by chromatographic methods to a high homogeneity. Suv3 eluted as a dimeric protein in the final size-exclusion chromatographic column (Superdex 200 10/300 column), whereas Suv3 $\Delta$ C eluted as a monomer when compared against the elution volume of standard proteins (Figure 1B). This result is consistent with a previous report showing that the crystal structure of a truncated form of Suv3 (residues 47–722) without the CTT folded as a monomer.<sup>6</sup> The molecular weights (MW) of Suv3 and Suv3 $\Delta$ C were determined by size exclusion chromatography-coupled multi-angle light scattering (SEC-MALS), which revealed a Suv3 MW of 148.6 kDa (calculated MW of dimeric Suv3 with a His-tag: 170 kDa), whereas Suv3 $\Delta$ C had a MW of 78.6 kDa (calculated MW of monomeric Suv3 with a His-tag: 85.3 kDa), confirming that Suv3 is a homodimer and Suv3 $\Delta$ C is a monomer (Figure 1C and D). These results verify that human Suv3 folds as a homodimer and that its CTT is required for dimerization.

### 2.2 | Suv3 preferentially binds to and unwinds duplex nucleic acids with a 3' overhang

Previous studies have revealed that human Suv3 displays helicase activity on multiple substrates, including RNA–RNA, RNA–DNA, and DNA–DNA duplexes,<sup>9</sup> and that it preferentially unwinds RNA–RNA duplexes with a 3' overhang.<sup>11</sup> To identify the optimal nucleic acid substrates for interactions with Suv3, we prepared various fluorophore-labeled single-stranded and double-stranded nucleic acid substrates to measure the dissociation constant between Suv3 and those substrates. We synthesized single-stranded DNA (ssDNA) and RNA (ssRNA) of 25 nucleotides (nt) in length with a 6-carboxyfluorescein (FAM) label at the 3' ends. These FAM-labeled nucleic acid substrates were incubated with various concentrations of Suv3 in the presence of the ATP analog AMPPNP and Mg<sup>2+</sup> ions, and then we measured the increasing fluorescence polarization (FP) signals to monitor protein–nucleic acid interactions (Figure 2A). Dissociation constants (Kd) were then calculated based on the assumption that one substrate is bound to one Suv3 protomer in a simple bimolecular binding reaction. Based on these FP assays, we found that Suv3 binds both ssDNA and ssRNA with high affinity, displaying a Kd of  $44.0 \pm 1.7$  nM for ssDNA and a Kd of  $53.1 \pm 0.7$  nM for ssRNA.

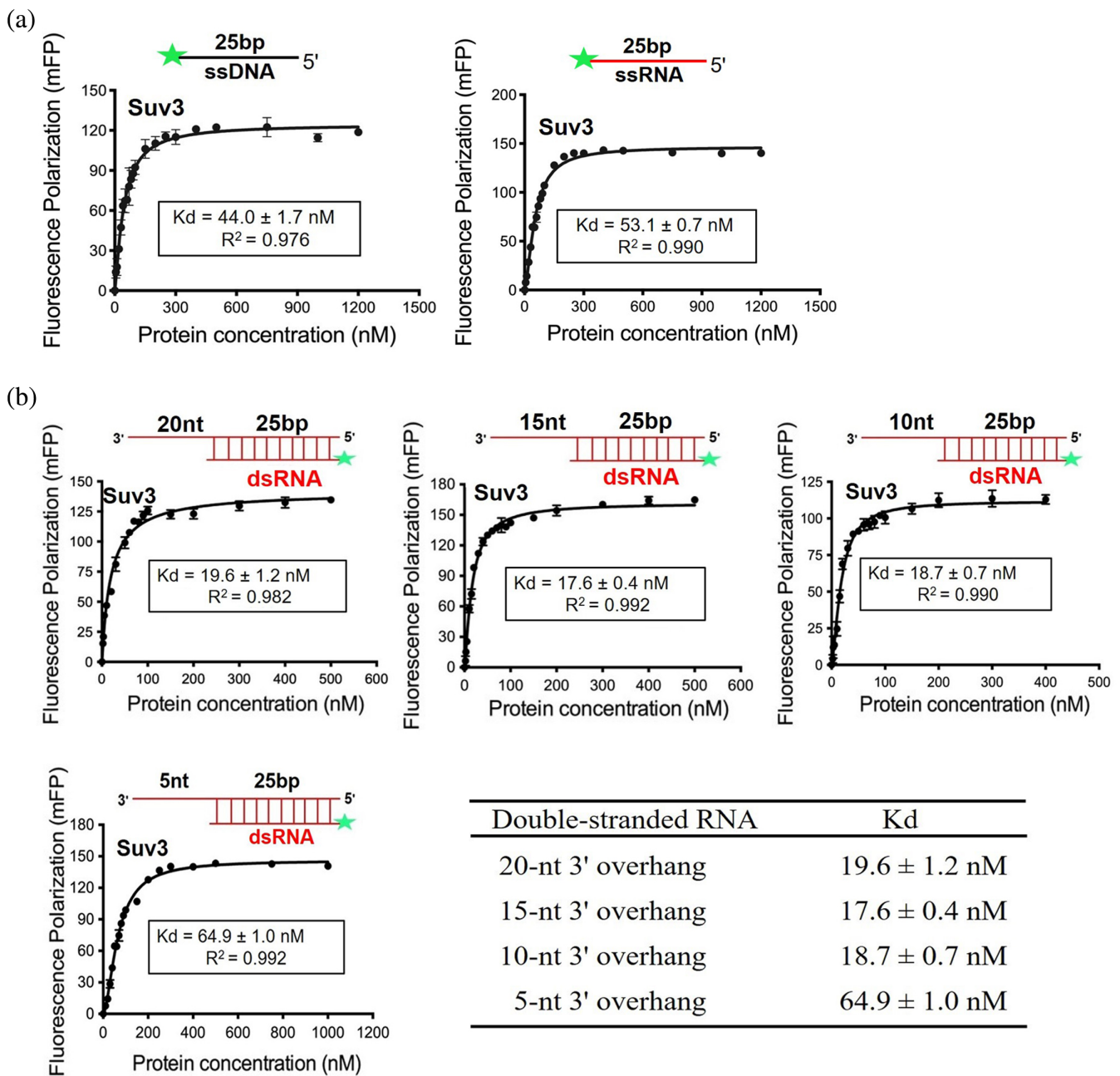


**FIGURE 2** Suv3 binds double-stranded RNA with a long 3' overhang ( $\geq 10$  nucleotides) with high affinity. (A) Binding affinities of Suv3 to single-stranded DNA (ssDNA) and RNA (ssRNA) were measured by fluorescence polarization (in mFP units) using 3'-end FAM-labeled 25-nt ssDNA and ssRNA as substrates. (B) Binding affinities of Suv3 to 3'-end FAM-labeled double-stranded RNA (dsRNA) with a 3'-overhang of 5, 10, 15, or 20 nucleotides. The fluorescence polarization signals were the average of three separate replicates, and error bars are shown in the figures representing one standard deviation. The dissociation constant (Kd) values were obtained by fitting the equations as shown in Materials and Methods

Next, we explored interactions between Suv3 and duplex nucleic acid substrates. We annealed FAM-labeled ssRNA with various complementary RNAs to generate dsRNAs bearing a 3' overhang of varying length (5, 10, 15, and 20 nt) (Figure 2B). We observed that Suv3 bound dsRNAs with long 3' overhangs of 10–20 nt with similarly low Kd values of  $\sim 18$  nM, whereas Suv3 bound less tightly to dsRNA with the short 5 nt 3'

overhang (Kd of  $\sim 65$  nM) (Figure 2B). This result demonstrates that Suv3 binds approximately two- to three-fold better to duplex nucleic acid substrates with a long 3' overhang ( $\geq 10$  nt) than to either single-stranded nucleic acids or duplex RNAs with a short 3' overhang, evidencing that both the long 3' overhang and the duplex region of the RNA substrates are involved in interactions with Suv3.

Next, we measured the binding affinity between Suv3 and dsDNAs, DNA–RNA hybrid duplexes, and dsRNAs with or without a 10-nt 3′ overhang or 5′ overhang (Figure 3). Suv3 bound with highest affinity to the substrates with 3′ overhangs, that is, dsDNA ( $K_d = 11.5 \pm 0.2$  nM), DNA–RNA hybrid ( $K_d = 13.1 \pm 0.4$  nM), and dsRNA ( $K_d = 18.7 \pm 0.7$  nM). In contrast, Suv3 bound blunt-end dsDNA ( $K_d = 63.9 \pm 1.5$  nM) and blunt-end DNA–RNA hybrid ( $K_d = 103.3 \pm 5.9$  nM) with a four to fivefold lower affinity relative to the duplex substrates hosting a 3′ overhang, while Suv3 bound most weakly to the blunt-end and 5′-overhang dsRNA substrates, with  $K_d$  values being below detection thresholds even when Suv3 concentration was increased to the micromolar range. Suv3 bound to DNA–DNA and DNA–RNA duplexes hosting a 10-nt 5′ overhang with respectively 8-fold and 23-fold lower affinities as compared with the ones with a 3′ overhang. The low  $K_d$  values in the nanomolar range between Suv3 and all three substrates with a 3′ overhang support that Suv3 binds to and unwinds such nucleic acid substrates in cellular environments. Notably, Suv3 does not bind blunt-end and 5′-overhang dsRNA, implying that Suv3 preferentially binds and unwinds duplex RNA with a 3′ overhang during mitochondrial RNA degradation.

We also performed helicase assays to explore if Suv3 unwinds 3′-FAM-labeled dsDNA, DNA–RNA hybrid, and dsRNA substrates with or without a 10-nt 3′ overhang. Suv3 was incubated with these different substrates in the presence of ATP and  $Mg^{2+}$  at 37°C for 1 hour before gel electrophoresis. Consistent with our binding assay results, we observed that duplex nucleic acid substrates hosting a 3′ overhang were unwound more efficiently in an ATP-dependent manner relative to the blunt-end substrates (Figure 4). Blunt-end dsDNA and DNA–RNA duplex could be unwound only at high Suv3 concentrations, whereas blunt-end dsRNA was not unwound by Suv3 even up to a concentration of 2  $\mu$ M (Figure 4). Taken together, these duplex binding and unwinding assays show that a 3′ overhang is crucial for Suv3 to tightly bind and efficiently unwind duplex substrates, including dsDNA, DNA–RNA hybrid, and dsRNA.

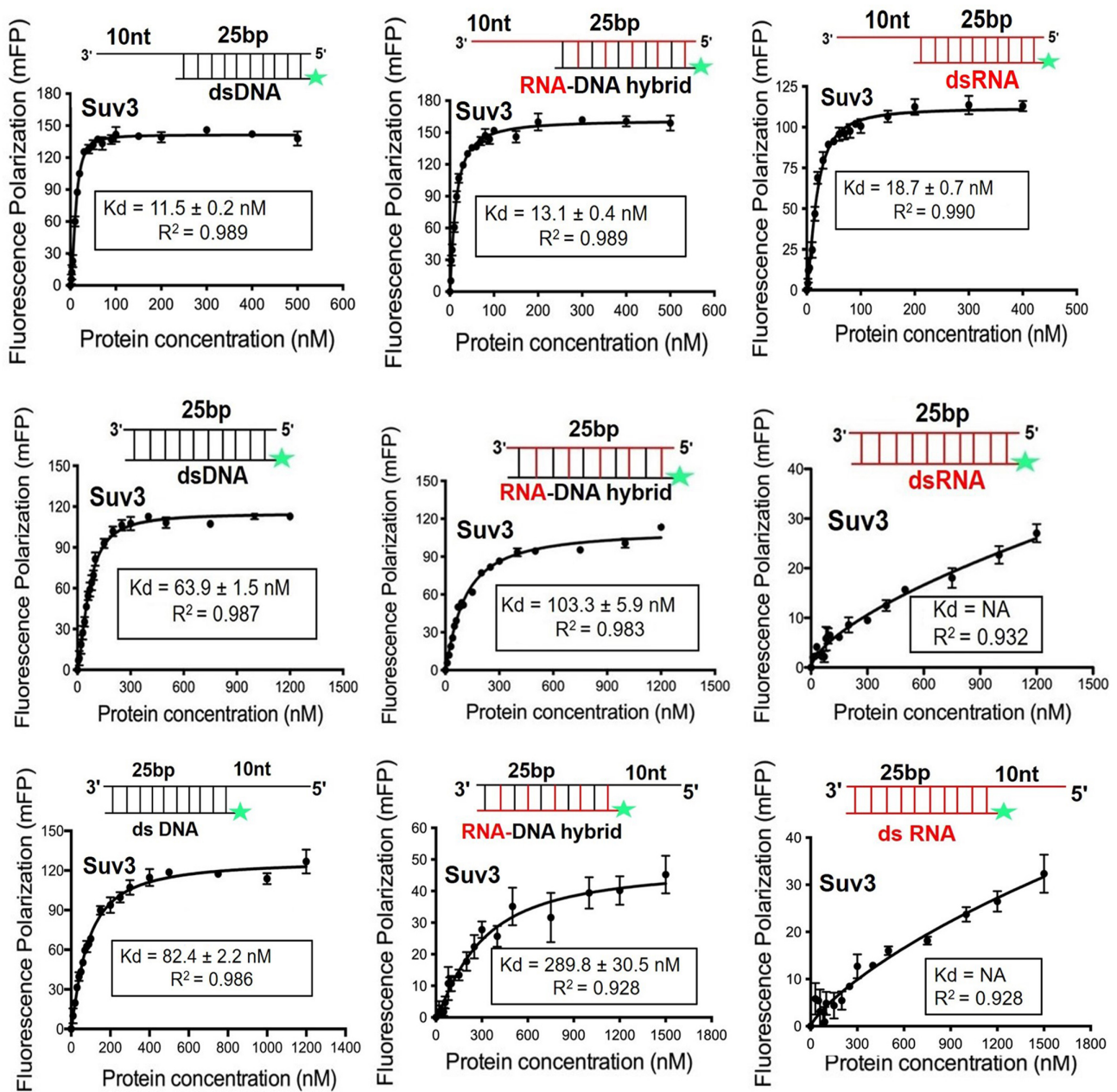
### 2.3 | Dimeric Suv3 assembly is crucial for strong RNA binding and efficient RNA unwinding activity

To further identify the functional importance of the Suv3 CTT in nucleic acid binding and unwinding activities, we tested interactions between Suv3 $\Delta$ C and dsDNA, DNA–RNA hybrid duplex, and dsRNA substrates with a 10-nt 3′ overhang. Fluorescence polarization assays revealed

that Suv3 $\Delta$ C bound these duplex 3′-overhang substrates with six to sevenfold lower binding affinities relative to those of Suv3 (dsDNA,  $K_d = 99.0 \pm 8.6$  nM; DNA–RNA hybrid,  $K_d = 110.2 \pm 9.5$  nM; dsRNA,  $K_d = 118.8 \pm 11.2$  nM) (Figure 5A). This result reveals that not only is the CTT of Suv3 required for dimerization, it is also necessary for the protein to strongly bind to its substrates. We further investigated the helicase activities of Suv3 $\Delta$ C and Suv3 against dsRNA substrate with a 10-nt 3′ overhang (Figure 5B). At the same concentrations of ATP (5 mM),  $Mg^{2+}$  (2 mM) and dsRNA (10 nM), Suv3 unwound the 3′ overhang dsRNA substrate more efficiently at lower concentrations ( $\geq \sim 30$  nM) than Suv3 $\Delta$ C ( $\geq \sim 120$  nM). Comparing the percentage of unwound RNA in that assay clearly demonstrated the significantly superior helicase activity of Suv3 over Suv3 $\Delta$ C (right panel in Figure 5B). The CTT (residues 723–786) of Suv3 does not share any sequence homology with other proteins and it contains a few basic amino acids. Secondary structure prediction by the GOR method<sup>31</sup> revealed that more than half of the regions in the CTT are disordered, with only two predicted  $\alpha$ -helices (Figure S1). Therefore, the CTT is likely involved in mediating interactions between Suv3 monomers to form dimeric protein. Combining the results of our nucleic acid binding and helicase assays, we conclude that the CTT is critical for Suv3 dimer formation and that dimeric assembly is required for Suv3 to exhibit strong binding to its substrates and to facilitate efficient RNA unwinding activity.

### 2.4 | Dimeric Suv3 binds RNA in an ATP- and ADP-independent manner

RNA helicases of SF2, such as DEAD-box helicases, typically remodel RNA by exhibiting different RNA-binding affinities during ATP hydrolysis cycles.<sup>3,32</sup> However, it was unclear how the RNA-binding activity of Suv3 is affected by ATP binding and hydrolysis. To answer this question, we performed fluorescence polarization assays on Suv3 and Suv3 $\Delta$ C in the presence or absence of the ATP analog AMPPNP (1 mM) or ADP (1 mM). We incubated dsRNA bearing a 10-nt 3′ overhang with Suv3, and observed similar  $K_d$  values for Suv3-bound dsRNA in the presence ( $K_d = 19.3 \pm 0.5$  nM) or absence ( $K_d = 32.6 \pm 0.6$  nM) of AMPPNP, as well as in the presence of ADP ( $K_d = 62.2 \pm 2.2$  nM) (Figure 6). In contrast, although Suv3 $\Delta$ C bound the dsRNA substrate with only a slightly lower affinity in the absence of AMPPNP ( $K_d = 224.2 \pm 9.2$  nM) than in its presence ( $K_d = 118.8 \pm 11.2$  nM), interactions between Suv3 $\Delta$ C and the dsRNA substrate were abrogated in the presence of ADP (Figure 6). These results indicate that only dimeric Suv3 allows RNA to



\*ND = Non detectable

**FIGURE 3** Suv3 preferentially binds duplex nucleic-acid substrates with a 3' overhang. Binding affinities of Suv3 to different duplex substrates, including DNA-DNA, DNA-RNA, and RNA-RNA, with a 10-nt 3' overhang (upper panel), no overhang (middle panel) or a 10-nt 5' overhang (lower panel). The fluorescence polarization signals were the average of three independent experiments, and error bars are shown in the figures representing one standard deviation.  $K_d$  values with standard deviation were obtained by fitting the binding curve to a one-site binding Hill-slope using Graph-pad Prism

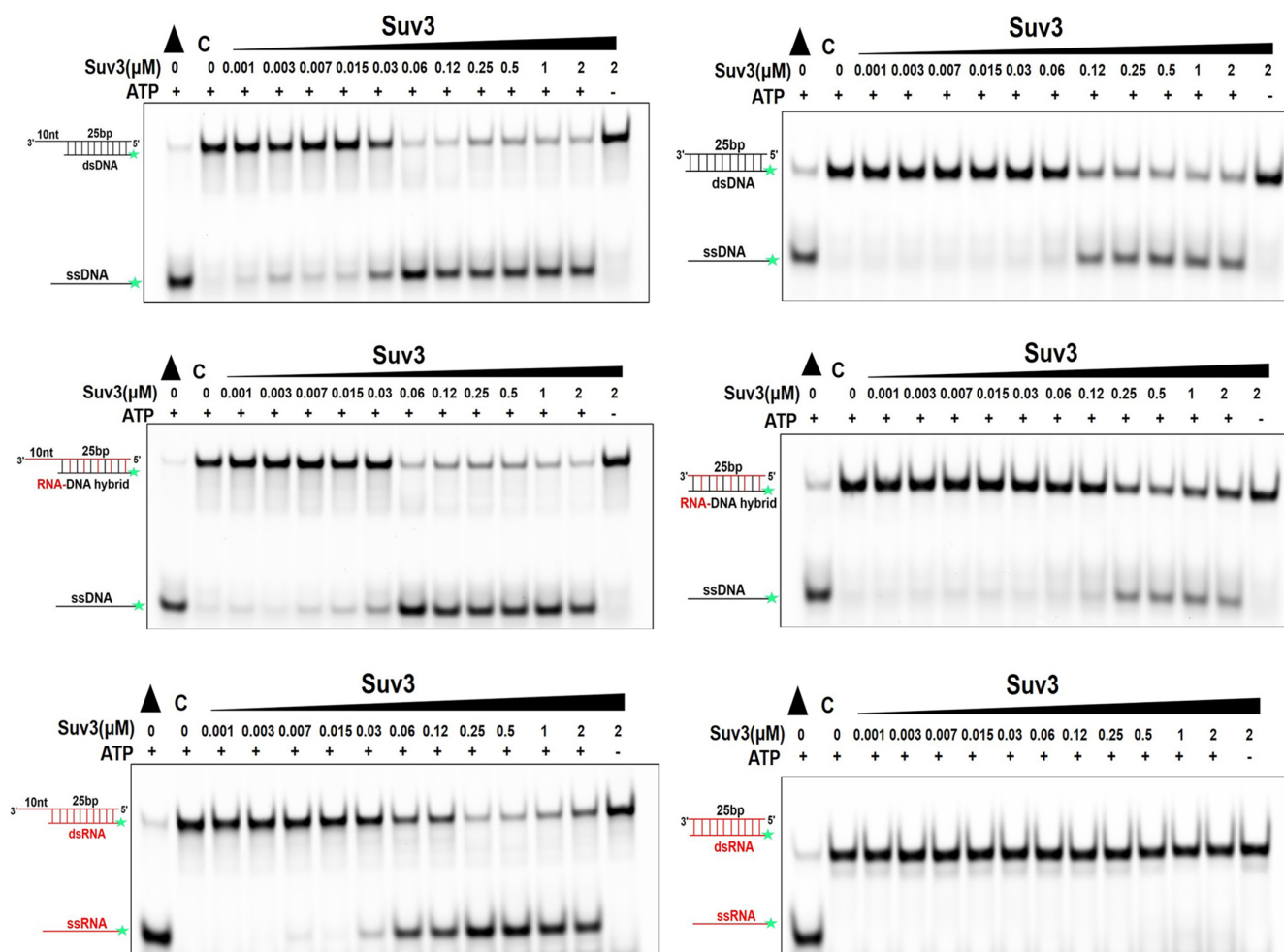


**FIGURE 4** Suv3 preferentially unwinds duplex substrates with a 3' overhang in an ATP-dependent manner. Increasing amounts of Suv3 were incubated with dsDNA, DNA–RNA hybrid, or dsRNA substrates, with or without a 10-nt 3' overhang, for 60 min at 37°C in the presence of ATP (5 mM). Duplex unwinding was resolved by 15% native PAGE with a starting Suv3 concentration of 2  $\mu$ M and subsequent serial two-fold dilution. Lane 1, black triangle denotes boiled substrates in which all double-stranded substrates were unwound after heating to 95°C for 5 min. Lane 2, C denotes control reaction in which no Suv3 was added and all substrates were annealed as duplexes. Suv3 displayed no unwinding activity in the absence of ATP and presented higher unwinding activity for duplex substrates with a 3' overhang (three left panels) compared with blunt-end duplexes (three right panels)

remain tightly bound upon ATP hydrolysis, since RNA appears to dissociate from monomeric Suv3 $\Delta$ C after ATP hydrolysis. Together, these findings show that Suv3 exhibits stronger RNA-binding activity than Suv3 $\Delta$ C and that RNA is continuously bound to dimeric Suv3 during ATP hydrolysis cycles.

## 2.5 | Crystal and SAXS structures of Suv3

To reveal the dimeric assembly of Suv3, we screened the crystallization conditions for the mature form of Suv3 in the absence or presence of ATP analog and ssDNA. After years of screening experiments, we did not obtain any

diffraction crystals of Suv3 dimer; however, we did crystallize the apo-form of Suv3 $\Delta$ C which diffracted X-ray to a resolution of 3.2 Å. The unit cell dimensions and space group of the apo-Suv3 $\Delta$ C was isomorphous to the monomeric Suv3-AMPPMP (residues 47–722, PDB ID: 3RC3) and Suv3–RNA complex (PDB ID: 3RC8). The structure of apo-Suv3 $\Delta$ C was refined using the template structure of Suv3-AMPPMP (PDB entry: 3RC3) as a starting model. The final structure of apo-Suv3 $\Delta$ C (PDB ID: 3RC3) revealed an empty ATP-binding site (Figure 7A and Table S1). The structure of apo-Suv3 fitted well with the structures of Suv3-AMPPMP and Suv3–RNA complex, giving an RMSD of 0.55 Å and 0.46 Å for 431 and 444 C $\alpha$  atoms, respectively (Figure 7C). Different from most of

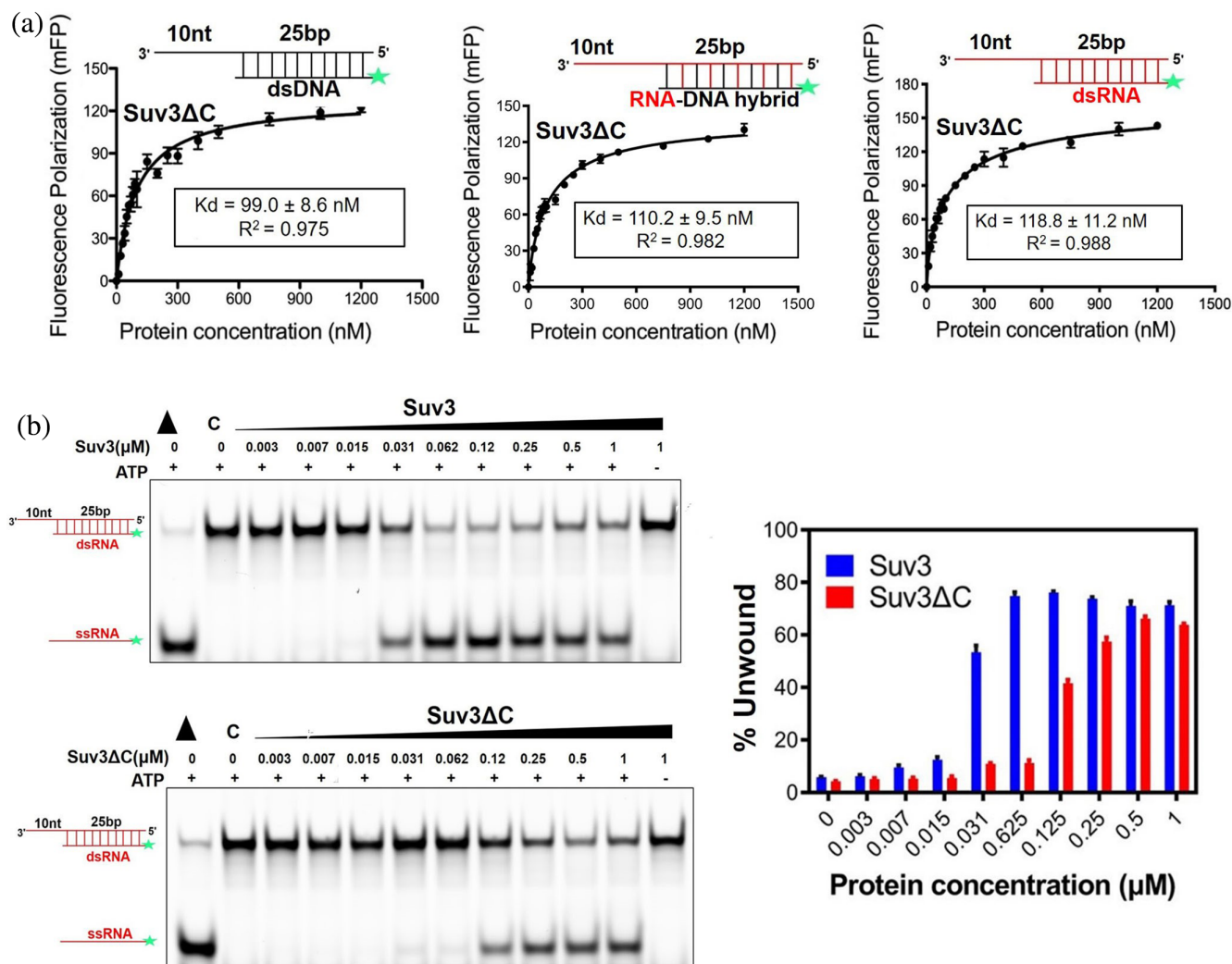


**FIGURE 5** CTT-truncated monomeric Suv3 (Suv3ΔC) displays lower RNA-binding and unwinding activities relative to dimeric Suv3. (A) Binding affinities of Suv3ΔC for 3'-end FAM-labeled dsDNA, DNA-RNA hybrid, and dsRNA substrates with a 10-nt 3' overhang were measured by fluorescence polarization. The K<sub>d</sub> values with standard deviation were obtained from three independent experiments. (B) RNA unwinding activities of Suv3 and Suv3ΔC with a starting concentration of 1 μM and a subsequent two-fold serial dilution in the presence of ATP are shown on 15% native PAGE. A comparison of the percentage unwound dsRNA by Suv3 and Suv3ΔC is shown in the right panel. Data represent mean of three independent experiments

the monomeric SF2-family RNA helicases, ssRNA and ATP binding to Suv3 does not induce an open to close conformational change between RecA1 and RecA2 domains, likely because the relative orientation of the two RecA domains is fixed by the CTD domain which bridges between the two RecA domains. We thus were able to construct a structural model revealing the AMPPNP- and RNA-binding sites between the two RecA domains in Suv3ΔC (Figure 7B). On the other hand, comparing to the structure of yeast Suv3 in the Suv3-Dss1 complex (PDB entry: 6F4A), NTD domain of yeast Suv3 shifts tremendously, suggesting that NTD domain of Suv3 might be flexible, and it may change its

conformation upon binding with exoribonuclease or RNA (Figure 7C).

To illustrate the dimeric assembly of Suv3, we further conducted small-angle X-ray scattering (SAXS) analysis on Suv3 and Suv3ΔC (Figure 7D). Analysis of the Guinier plots and pair-distribution functions revealed a gyration radius (R<sub>g</sub>) of 35.4 Å and a maximum diameter (D<sub>max</sub>) of 120 Å for Suv3ΔC, and an R<sub>g</sub> of 46.8 Å and a D<sub>max</sub> of 185 Å for Suv3 (Figure 7D and E). The molecular weights estimated by SAXS were 78.2 kDa for Suv3ΔC and 148.6 kDa for Suv3, that were in close agreement with the molecular weights estimated from SEC-MALS (shown in Figure 1). We also performed SAXS on Suv3 in



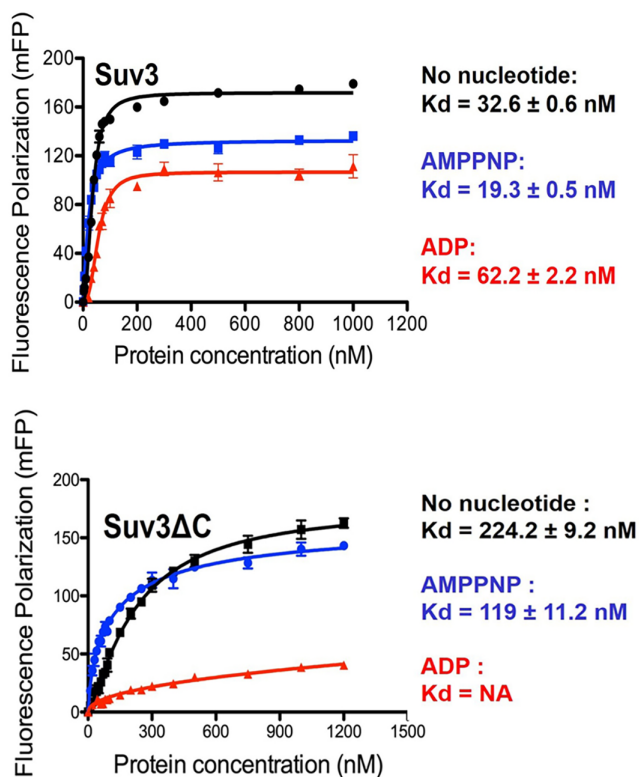


**FIGURE 6** Dimeric Suv3 binds RNA substrates in an ATP- and ADP-independent manner. RNA-binding affinities of Suv3 and Suv3ΔC for double-stranded RNA with a 10-nt 3' overhang were measured by fluorescence polarization assays in the presence or absence of 1 mM AMPPNP or ADP. Data represent Suv3 and Suv3ΔC activity in the presence of AMPPNP (blue circles), the presence of ADP (red triangles), and the absence of nucleoside (black squares). Respective Kd values with standard deviation for plot fitting are shown at right

the presence of AMPPNP and ssDNA, which resulted in a slightly reduced Rg of 44.8 Å and a Dmax of 160 Å compared with those calculated for Suv3 alone. The dimensionless Kratky plot of Suv3-AMPPNP-ssDNA also suggests a less flexible globular assembly as compared with the one of Suv3 alone (Figure 7E). Together, these results imply a more compact conformational change for Suv3 dimer upon binding of AMPPNP and ssDNA (Figure 7E).

We further calculated the ab initio electron density maps of Suv3ΔC (p1 symmetry) and Suv3 (p2 symmetry) by DENSS<sup>33</sup> (Figure 7F). Fourier shell correlation (FSC) curve from DENSS reconstruction estimated a resolution of 29.0 Å for Suv3ΔC, 33.5 Å for apo-form of Suv3, and 48.4 Å for Suv3-AMPPNP-ssDNA complex (Figure S2A). Plots of experimental intensity fitted reasonably well with the calculated intensities from DENSS map of Suv3ΔC, Suv3, and Suv3-AMPPNP-ssDNA (Figure S2B). The

crystal structure of the apo-form of monomeric Suv3ΔC determined in this study fitted comparably in size and shape into the envelope of Suv3ΔC (Figure 7F). For the structural envelop of Suv3 dimer, we manually fitted two Suv3 monomers into the envelope so that their NTDs oriented outwards, whereas their CTDs and CTTs faced inward to form the dimerization interface. This model of the Suv3 dimer thus agrees with our biochemical analyses showing that CTT located in the C-terminal end of Suv3 is required for Suv3 dimerization. We also deployed the ab initio modeling methods of GASBOR<sup>34</sup> and DAMMIN<sup>35</sup> for shape determination of Suv3ΔC, Suv3, and Suv3-AMPPNP-ssDNA. Envelope structures of Suv3ΔC, Suv3, and Suv3-AMPPNP-ssDNA complex generated by GASBOR and DAMMIN revealed similar sizes and shapes to the ones generated by DENSS (Figures S3 and S4). These consistent results support that apo-form of Suv3 dimer is assembled into a football-shaped structure with a dimension of 185 × 95 × 83 Å<sup>3</sup>.

## 2.6 | Monomeric Suv3ΔC cannot interact with PNPase to form mitochondrial degradosome

To determine how human Suv3 forms a complex with PNPase, we expressed and purified the mature form of PNPase (residue 46–783) without the N-terminal mitochondrial localization sequence by chromatographic methods. The C-terminal His-tagged PNPase formed a stable trimeric protein as reported previously.<sup>36</sup> To reconstitute the Suv3-PNPase complex, Suv3 and PNPase were mixed in the complex assembly buffer containing 25 mM potassium phosphate pH 8.0, 300 mM KCl, 1 mM MgCl<sub>2</sub>, 2 mM DTT, and 10% glycerol in the 2:3 M ratio at 4°C overnight. The size of the Suv3-PNPase complex was analyzed by gel filtration chromatography (Superose 6 10/300 GL column) revealing a monodispersed peak containing the two proteins as shown in the SDS-PAGE (Figure 8A). In contrast to the dimeric Suv3, monomeric Suv3ΔC (residues 48–722) and PNPase after incubation in the complex assembly buffer at 4°C overnight were eluted as two separated peaks in the gel filtration chromatography, indicating no complex was formed. Suv3ΔC and PNPase were eluted at different fractions as shown in SDS-PAGE, confirming that Suv3ΔC could not form a complex with PNPase (Figure 8B).

We next tested the exoribonuclease activities of PNPase in degrading duplex RNA in the presence of Suv3 or Suv3ΔC. We incubated the 5'-end FAM-labeled 20-nt dsRNA with a 20-nt 3' overhang with PNPase and Suv3 in the degradation buffer. PNPase barely degraded

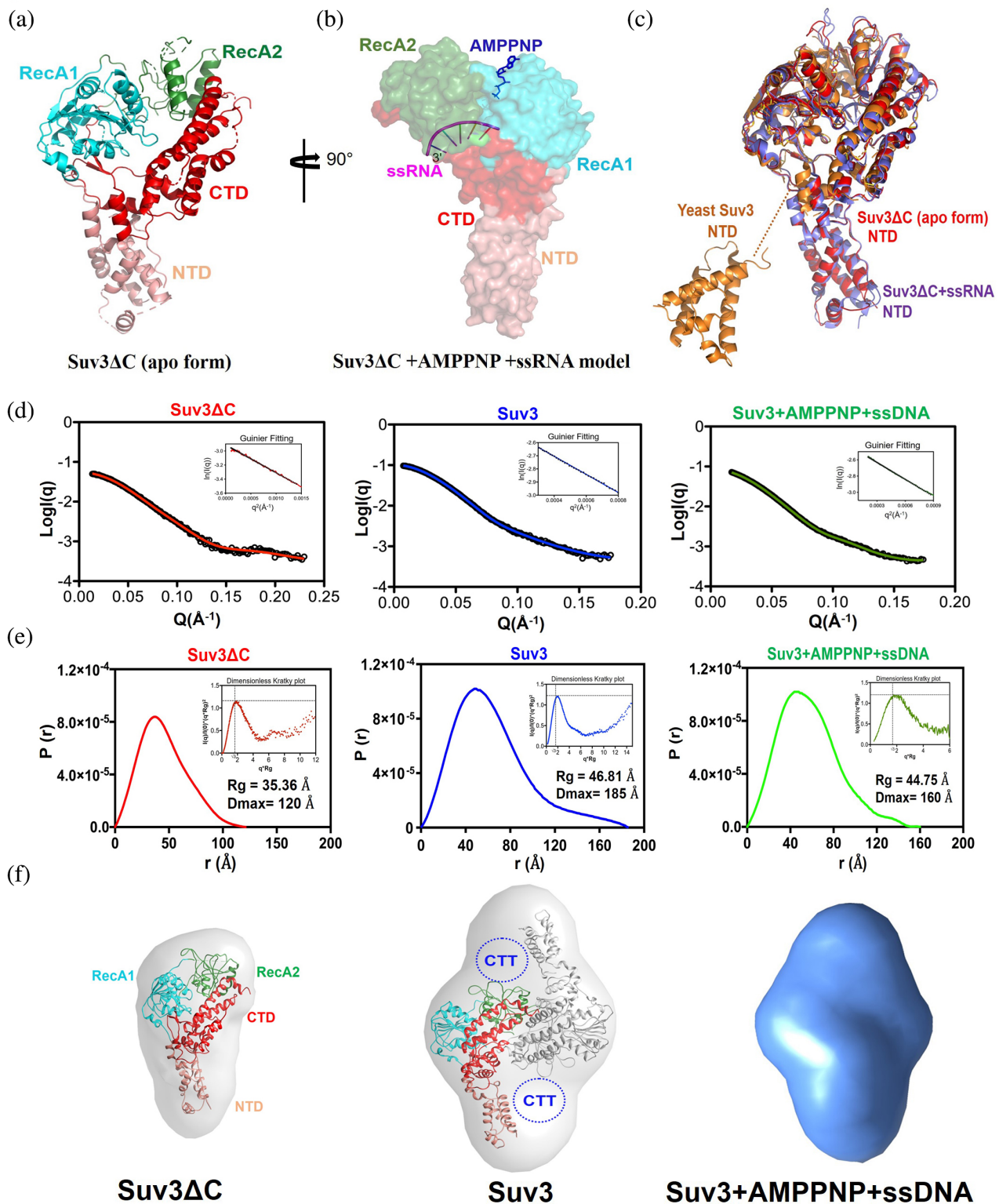


**FIGURE 7** Crystal and SAXS structures of Suv3. (A) The crystal structure of apo-form of Suv3ΔC (PDB ID: 7W1R). (B) Structural model of Suv3ΔC bound with AMPPNP (in blue) and ssRNA (in magenta). (C) Superimposition of the crystal structures of apo-form Suv3ΔC (in red), Suv3–RNA complex (in light blue, PDB ID: 3RC8), and yeast Suv3 (in orange, PDB ID: 6F4A) reveals that NTD of Suv3 is flexible. (D) SAXS scattering curves and Guinier plots of Suv3ΔC (in red), Suv3 (in blue) and Suv3-AMPPNP-ssDNA (in green). Theoretical scattering intensities generated for envelopes shown in (F) are displayed in black lines which are fitted well to the experimental curves. (E) Distance distribution functions and Kratky plots of Suv3ΔC (in red), Suv3 (in blue) and Suv3-AMPPNP-ssDNA (in green) reveal the maximum diameters of the protein molecules (generated from GNOM of the ATSAS package). (F) Ab initio maps from SAXS data of Suv3ΔC, Suv3 dimer and Suv3-AMPPNP-ssDNA were generated with DENSS. The crystal structure of Suv3ΔC (apo form) determined in this study was fitted into the SAXS envelope. The location of CTT is marked as a dashed circle in the structure of Suv3 dimer

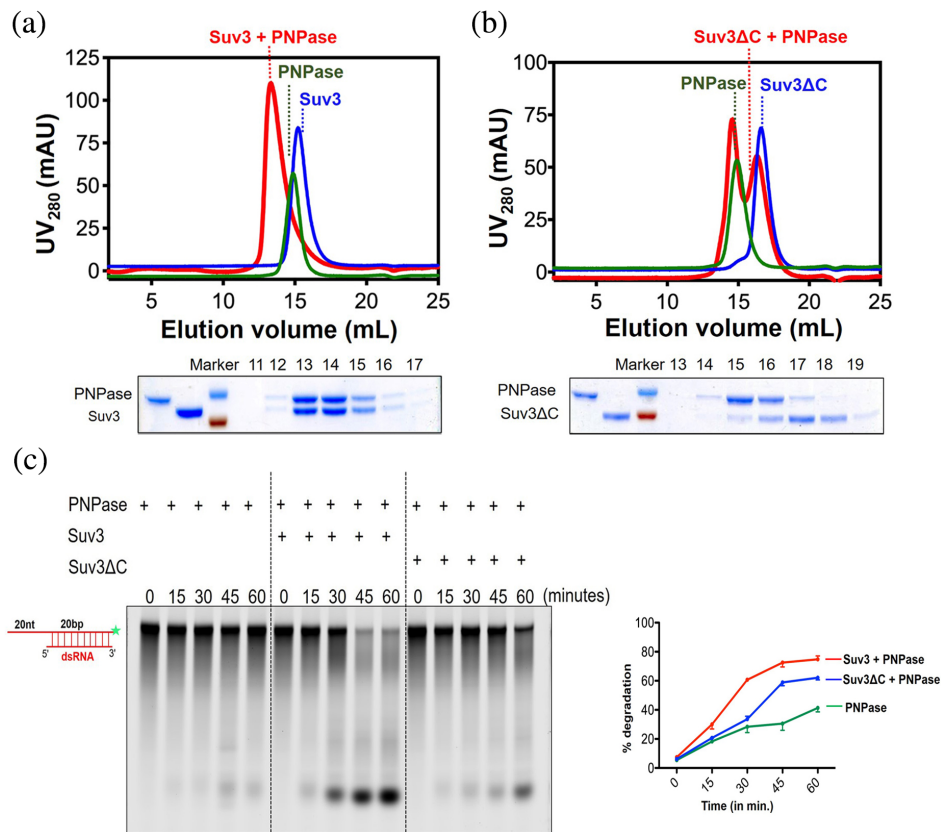


**FIGURE 8** Dimeric Suv3 but not monomeric Suv3ΔC can interact with PNPase to form mitochondrial degradosome. (A) Gel filtration (Superose 6 10/300 GL) elution profiles of Suv3 (blue), PNPase (green), and Suv3–PNPase complex (red) reveal that Suv3–PNPase forms a monodispersed complex in 2:3 M ratio. SDS–PAGE analysis of elution fractions is shown in the lower panel. (B) Gel filtration (Superose 6 10/300 GL) elution profile of Suv3ΔC (blue), PNPase (green), and Suv3ΔC + PNPase (red) reveal that monomeric Suv3ΔC cannot form a complex with PNPase. (C) Time course of RNA degradation assays of PNPase alone, Suv3 + PNPase and Suv3ΔC + PNPase reveal that Suv3–PNPase complex (10 nM) degraded 5′-FAM-labeled dsRNA with a 20-nt 3′ overhang more efficiently than Suv3ΔC + PNPase and PNPase alone. A comparison of the percentage of dsRNA substrate that were degraded by PNPase alone, Suv3–PNPase, and Suv3ΔC + PNPase in the time-course experiments is shown in right panel. Data represent mean of three independent experiments

dsRNA substrates in the time-course experiment, but with the addition of Suv3, dsRNA was degraded efficiently by the mixture of PNPase and Suv3 (Figure 8C). On the other hand, dsRNA was degraded slightly better by the mixture of PNPase and monomeric Suv3ΔC as compared with PNPase alone (Figure 8C). Combining all these results suggests that only Suv3 dimer is capable of interacting with PNPase and effectively promoting the exoribonuclease activity of PNPase in RNA degradation.

## 2.7 | Dimeric Suv3 forms a dumbbell-like complex structure with PNPase

To elucidate the overall assembly structure of Suv3–PNPase complex, the solution structure of Suv3–PNPase complex in the presence of AMPPNP was determined by SAXS. The SAXS profiles were recorded for full-length PNPase and Suv3–PNPase complex (Figure 9A). Analysis

of Guinier plots and pair distance distribution functions of PNPase revealed a gyration radius ( $R_g$ ) of 45.7 Å and a maximum diameter ( $D_{max}$ ) of 177 Å, whereas Suv3–PNPase complex had an  $R_g$  of 77.9 Å and  $D_{max}$  of 320 Å. The Kratky plot of Suv3–PNPase complex suggested a well folded multidomain assembly with partially flexible regions (Figure 9B). Fourier shell correlation (FSC) curve from DENSS reconstruction estimated a resolution of 32.4 Å for PNPase, and 51.9 Å for Suv3–PNPase complex (Figure S5).

The ab initio electron density maps of PNPase generated by DENSS (p3 symmetry) revealed a funnel-like structure with the three S1 domains associated on the top of the PNPase degradation chamber, in agreement with the crystal structure of the full-length *Caulobacter crescentus* PNPase.<sup>37</sup> The ab initio electron density map for Suv3–PNPase complex (p1 symmetry) revealed a dumbbell-shaped structure (Figure 9C). Similar shaped models of PNPase and Suv3–PNPase complex were

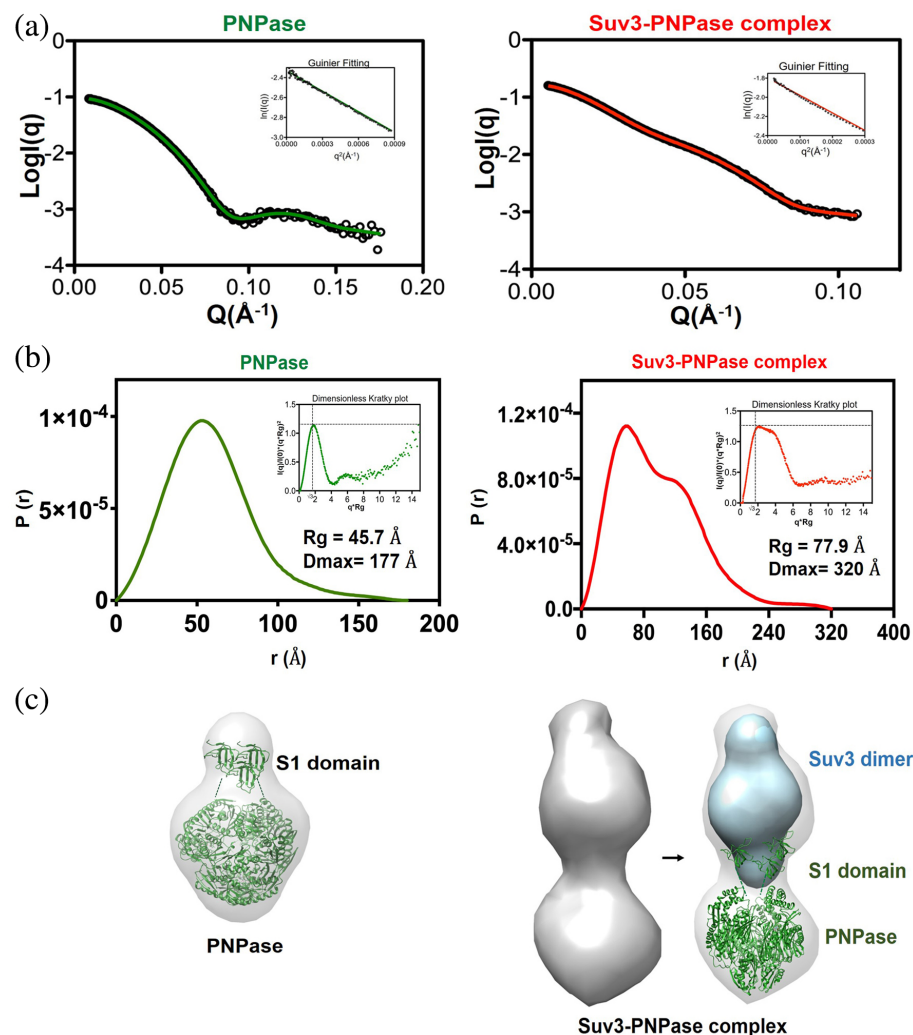


**FIGURE 9** Dimeric Suv3 forms a dumbbell-like complex structure with PNPase. (A) SAXS scattering curves of PNPase (in green) and Suv3–PNPase complex (in red) are represented as logarithmic scattering intensities. Theoretical scattering intensities (in black) generated for envelopes shown in (C) are fitted to the experimental curves. (B) Distance distribution functions reveal the maximum diameters of the protein molecules (generated from GNOM of the ATSAS package), whereas Kratky plots of PNPase and Suv3–PNPase complex suggest these proteins are well folded in solution with partial flexible regions. (C) Ab initio maps from SAXS data of PNPase and Suv3–PNPase were generated with DENSS. The SAXS envelop of Suv3 dimer (in light blue) and the crystal structure of human PNPase trimer (displayed in green ribbon model, PDB ID: 3U1K) are well fitted into the SAXS map of Suv3–PNPase complex, revealing a dumbbell-shaped structure. The S1 domain of PNPase is highly flexible, so its location in this figure is slightly different from the ones shown in the Figures S6 and S7

generated by GASBOR and DAMMIN with low  $\chi^2$  values (Figures S6 and S7). We thus conclude that dimeric Suv3 caps on the top of PNPase via interactions with S1 domains, and forms a dumbbell-shaped degradosome complex with PNPase for efficient RNA unwinding and degradation.

### 3 | DISCUSSION

We have shown herein that human Suv3 is a homodimer, whereas CTT-truncated Suv3 $\Delta$ C is monomeric. Suv3 must dimerize to exhibit strong substrate binding and to conduct efficient unwinding of duplex substrate hosting a 3' overhang. That Suv3 dimer preferentially unwinds duplex RNA with a 3' overhang is in agreement with a previous study showing that human Suv3–PNPase complex more efficiently degrades dsRNA with a 3' overhang than the same substrate with a 5' overhang.<sup>11</sup> The crystal structure of Suv3 $\Delta$ C shows that its NTD and CTD fold similarly to the 1B and 2B domains

of UvrD or PcrA, which likely participate in RNA binding.<sup>38</sup> However, how the CTT of Suv3 folds and its function had remained ambiguous. Based on our biochemical data, we suggest that the CTT of Suv3 is a dimerization motif that plays a key role in maintaining the dimeric assembly of Suv3.

Apart from its activity on dsRNA, we have also shown that Suv3 dimer can efficiently unwind RNA–DNA and DNA–DNA duplexes with a 3' overhang. This result is consistent with the previous finding that Suv3 is involved in resolving RNA–DNA duplex to prevent R-loop formation during transcription.<sup>22</sup> Suv3 may also play a key role in resolving dsDNA in DNA repair and/or replication pathways in mitochondria, as low-level Suv3 expression results in increased numbers of mtDNA mutations and decreased mtDNA copy numbers, reflecting genome instability.<sup>19</sup> Consequently, our results support that Suv3 may display multiple functions, not only acting to unwind RNA–RNA duplex in RNA decay pathways, but also relaxing RNA–DNA and DNA–DNA duplexes in other metabolic processes of RNA and DNA in mitochondria.

Together, human dimeric Suv3 and trimeric PNPase constitute the mitochondrial degradosome for efficient RNA turnover in mitochondria.<sup>11</sup> This 2-to-3 assembly of helicase and PNPase has also been observed in bacterial minimal RNA degradosomes, including *E. coli* PNPase–RhIB complex and *B. subtilis* PNPase–CshA complex.<sup>25–27</sup> The RNA-degrading machinery comprising trimeric PNPase and a dimeric helicase is thus conserved from bacteria to human. Since monomeric Suv3 $\Delta$ C is still an active helicase, it is intriguing why Suv3, and all of the helicases associated with PNPase, have to be homodimers. Our biochemical assays reveal that only dimeric Suv3 can bind RNA substrates independently of ATP and ADP, suggesting that RNA remains continuously associated with Suv3 during ATP hydrolysis, that is, RNA-bound Suv3 can enter another ATPase cycle upon ADP release. These results are similar to those reported for the dimeric DEAD-box helicase CshA, which also binds RNA in an ATP- and ADP-independent manner.<sup>29</sup> Since PNPase is a processive exoribonuclease, RNA is continuously associated with it during the process of removing one nucleotide at a time from the 3' to 5' ends.<sup>39</sup> Dimeric Suv3 may ensure continuous RNA binding and unwinding during the RNA degradation process of PNPase–Suv3 complex. Thus, our results explain why Suv3 has to dimerize so it can interact and work cooperatively with a processive PNPase. Accordingly, the mitochondrial degradosome represents a highly efficient compact machinery for cooperative and processive RNA binding, unwinding, and degradation. Our SAXS analysis reveals the dimeric assembly of Suv3, showing how this helicase may form a dimer via its CTT, and how it forms a dumbbell-shaped complex with PNPase. However, the detailed mechanisms of RNA binding and unwinding by Suv3 remain elusive and await high-resolution structural investigation.

## 4 | MATERIALS AND METHODS

### 4.1 | Protein expression and purification

The cDNAs of full-length human Suv3 (residues 48–786) and Suv3 $\Delta$ C (residues 48–722) without the MLS were PCR-amplified and sub-cloned into pET15b vector to express the respective recombinant proteins with an N-terminal His-tag. The N-terminal His-tag Suv3 and Suv3 $\Delta$ C constructs were transformed into the *Escherichia coli* strain Rosetta (DE3) (Novagen). The transformed cells were grown in LB medium at 37°C, and protein expression was induced for 18 h at 18°C with 0.8 mM IPTG when OD<sub>600</sub> reached 0.5–0.8. Cells were then harvested by centrifugation and all subsequent

experiments were performed at 4°C. The harvested cells were lysed by microfluidizer (Microfluidics M-110) in lysis buffer containing 50 mM Tris–HCl pH 8.0, 1 M NaCl, and 10 mM imidazole. The lysate was clarified by centrifugation for 30 min at 17,000 rpm. Recombinant His-tagged Suv3 and Suv3 $\Delta$ C were purified by chromatographic methods, using HisTrap FF (5 mL, GE HealthCare), Heparin HP (5 mL, GE HealthCare), and Superdex 200 16/600 (GE HealthCare) columns. Purified His-tagged proteins were concentrated to 5 mg/mL and stored at –80°C in the storage buffer of 20 mM HEPES pH 7.8, 300 mM NaCl and 2 mM DTT.

The cDNA of the full-length human PNPase without its MLS (residues 46–783) was cloned into the expression vector pET28b (Novagen) to express recombinant proteins with a C-terminal His-tag. The C-terminal His-tag PNPase construct was transformed into the *Escherichia coli* strain B834 (Stratagene). After transformation, induction, cell harvesting, and cell lysis, recombinant His-tagged PNPase was purified by chromatographic methods, using HisTrap FF (5 mL, GE HealthCare), HiTrap Heparin HP (5 mL, GE HealthCare), Phenyl HP (5 mL, GE Healthcare), and Superdex 200 10/300 (GE HealthCare) columns. Purified His-tagged proteins were concentrated to 8–10 mg/mL and stored at –80°C in the storage buffer of 20 mM HEPES pH 7.8, 300 mM NaCl, and 2 mM DTT.

### 4.2 | Size exclusion chromatography coupled with multi-angle light scattering (SEC-MALS)

Molecular weights of Suv3 and Suv3 $\Delta$ C were measured by SEC-MALS. S200 10/300 columns connected to a DAWN HELIOS II-18 angle MALS (Wyatt Technology) detector with wavelength set at 658 nm were equilibrated in 25 mM HEPES pH 8.0, 300 mM KCl, and 2 mM DTT and with a flow rate of 0.2 mL/min using the ÄKTA-UPC 900 FPLC system (GE Healthcare). Purified protein samples were centrifuged at high speed for 15 min at 4°C and filtered through a 0.22- $\mu$ m filter (Millipore). Protein samples (100  $\mu$ L injection volumes) were injected into the Superdex S200 10/300 columns. UV fluorescence, MALS, and Refractive Index data were recorded and analyzed using ASTRA software (Wyatt Technology).

### 4.3 | Nucleic acid substrate binding assays

All RNA oligomers and DNA oligomers were synthesized and purified by MdBio Inc. and Mission Biotech,

respectively. The 3'-end FAM-labeled 25-nt RNA was mixed with an equimolar amount of different lengths of RNA in annealing buffer containing 20 mM Tris-HCl pH 7.0, 100 mM NaCl, and 1 mM EDTA, and then heated to 95°C for 5 min followed by slow cooling at room temperature to generate duplex RNA substrates hosting different 3'-end overhangs of 20, 15, 10, or 5 nucleotides. Similarly, 3'-end FAM-labeled 25-nt DNA was annealed with an equimolar mixture of DNA or RNA to generate the DNA-DNA and DNA-RNA hybrid duplexes with a 10 nt 3'-end overhang. Also, the 10-nt 5'-overhang duplex substrates and blunt-end DNA-DNA, RNA-RNA or DNA-RNA hybrid substrates were prepared using the same procedure. The DNA-DNA and DNA-RNA duplexes used in fluorescence polarization assays and helicase assays were prepared by annealing:

5'-GGTGTGGTGGCATACTGCAGACGC-FAM with.  
5'-GCGTCTGCACGTATGCCACCACACC-3' or.

5'-GCGTCTGCACGTATGCCACCACACCAGGAGAG  
GAG-3' and.

5'-GAGGAGAGGAGCGTCTGCACGTATGCCACCA  
CACC-3'.

to generate DNA-DNA duplex with blunt-end or a 10-nt 3' and 10-nt 5' overhang, respectively. The DNA-RNA hybrid duplexes were prepared by annealing 5'-GGTGTGGTGGCATACTGCAGACGC-FAM with.

5'-GCGUCUGCACGUAUGCCACCACACC-3', or.

5'-GCGUCUGCACGUAUGCCACCACACCAGGAGA  
GGAG-3', and.

5'-GAGGAGAGGAGCGUCUGCACGUAUGCCACC  
ACACC-3' to generate the DNA-RNA hybrid duplex with blunt-end or with a 10-nt 3' and 10-nt 5' overhang, respectively. The RNA-RNA duplexes were prepared by annealing.

5'-GGUGUGGUGGCAUACGUGCAGACGC-FAM with.

5'-GCGUCUGCACGUAUGCCACCACACC-3',

5'-GCGUCUGCACGUAUGCCACCACACCAGGAG-3',

5'-GCGUCUGCACGUAUGCCACCACACCAGGAG  
AGGAG-3',

5'-GCGUCUGCACGUAUGCCACCACACCAGGAG  
AGGAGAGGAG-3', or.

5'-GCGUCUGCACGUAUGCCACCACACCAGGAG  
AGGAGAGGAGAGGAG-3' and.

5'-GAGGAGAGGAGCGUCUGCACGUAUGCCACC  
ACACC-3' to generate RNA-RNA duplexes with 3'-end overhangs of 0, 5, 10, 15, or 20 nucleotides, and 10-nt 5' overhang respectively.

Binding affinities of recombinant Suv3 and Suv3ΔC proteins with multiple single-stranded and double-stranded substrates were estimated based on increasing fluorescence polarization (FP) signals, as monitored by a paradigm plate reader (Molecular Devices). The 3'-

overhang duplex substrates (1 nM) and the blunt-end and 5'-overhang duplex substrates (10 nM) were respectively mixed with the indicated concentration of proteins in binding buffer containing 20 mM Tris-HCl pH 7.5, 50 mM KCl, 0.1 mM EDTA, 2 mM MgCl<sub>2</sub>, 1 mM DTT, 100 μg/mL BSA, 10% glycerol, and 1 mM AMPPNP. Protein and substrates were incubated for 20 min at room temperature and FP signals were excited at 485 nM and read at 538 nM. Dissociation constant (K<sub>d</sub>) values were calculated by plotting FP values against protein concentration and fitting the binding curve to a one-site binding Hill slope using GraphPad Prism 9 software.

Fluorescence polarization (FP) values were calculated using Equation (1), where *I*<sub>para</sub> and *I*<sub>perp</sub> represent the fluorescent intensities of signals in the parallel and perpendicular planes, respectively. The calculated FP values were plotted against Suv3 concentrations and the binding curves were fitted to obtain K<sub>d</sub> values using Equation (2).

$$mFP = 1000 \times \frac{[I_{para} - I_{perp}]}{[I_{para} + I_{perp}]} \quad (1)$$

$$y = FP_{min} + \frac{FP_{max} - FP_{min}}{1 + \left(\frac{x}{Kd}\right)^n} \quad (2)$$

#### 4.4 | Measuring the helicase activity of Suv3

Duplex unwinding assays were performed at 37°C in 10 μL reaction buffer containing 20 mM HEPES pH 7.0, 50 mM KCl, 2 mM MgCl<sub>2</sub>, 1 mM DTT, 5% glycerol, 0.1% Triton X-100, and 50 nM cold RNA or DNA oligomer. Annealed substrates (10 nM) were incubated with increasing concentrations of recombinant Suv3 or Suv3ΔC protein for 10 min at 4°C, and the unwinding reactions were initiated by adding 5 mM ATP at 37°C. Reactions were quenched after 1 h by adding 5 μL of stop buffer containing 20 mM HEPES pH 7.4, 300 mM KCl, 10 mM EDTA, and 200 ng/μl proteinase K for 1 h at 37°C. All samples were resolved in 15% native TBE gel, imaged using a Typhoon FLA 9000 scanner (GE Healthcare), and quantified in Image J software.

#### 4.5 | Crystal structure determination and refinement of Suv3ΔC

Suv3ΔC (apo-form) was crystallized by the hanging drop vapor diffusion method at 20°C by mixing 1 μL of protein sample (5 mg/mL in 20 mM HEPES pH 7.4, 300 mM KCl, and 2 mM DTT), and 1 μL of reservoir solution (0.005 M magnesium sulfate heptahydrate, 0.05 M MES

monohydrate pH 6.0 and 5% w/v polyethylene glycol 4,000). X-ray diffraction data were collected at BL44XU beamline at SPring-8, Harima, Japan. The collected data were processed and scaled by HKL2000. The crystal structure of Suv3 $\Delta$ C was refined by Phaser in PHENIX program employing Suv3-AMPPNP complex crystal structure (PDB ID: 3RC3) as the search model. Structural model was built using Coot program and refined in PHENIX. All the data collection and structural refinement statistics are listed in Table S1.

#### 4.6 | Small angle X-ray scattering (SAXS) data collection and analysis

For SAXS experiments, Suv3 $\Delta$ C, Suv3, PNPase, and Suv3-PNPase complex were purified to high homogeneity and then concentrated to 4–5 mg/mL in 20 mM HEPES buffer, 300 mM KCl, 2 mM MgCl<sub>2</sub>, 2 mM DTT, and 5% glycerol. For Suv3-AMPPNP-ssDNA complex, purified Suv3 was incubated with 1 mM AMPPNP and a 1:2 M ratio of Suv3 and DNA. All protein samples and protein complexes were freshly purified prior to SAXS measurements so as to avoid freeze-thaw cycle. SAXS data were recorded at SAXS beamline TPS-13A coupled to an Agilent-Bio SEC-3300 Å column in the National Synchrotron Radiation Research Center, Hsin-Chu, Taiwan. SAXS data were collected at an X-ray wavelength of about 1 Å and an energy of 15Kev for all samples. The sample-to-detector distance for Suv3 $\Delta$ C and Suv3 was 2.5 m while for PNPase and Suv3-PNPase complex was 3.6 m. Frames collected for Suv3 $\Delta$ C and Suv3 was 136, for PNPase was 120 frames, and for Suv3-PNPase complex was 200 frames of 2 s exposure. Selected frames after merging were used to estimate initial R<sub>g</sub> in the Primus program.

The BioXTAS RAW<sup>40</sup> and ATSAS software<sup>41</sup> package were used for SAXS data processing and analysis. The P<sub>r</sub> distance distribution and D<sub>max</sub> was analyzed using GNOM.<sup>42</sup> Molecular weight of all protein samples from SAXS data was determined by porod volume and volume of correlation (V<sub>c</sub>). Low-resolution ab initio envelope of protein and protein-complex was generated by DAMMIN<sup>35</sup> and GASBOR<sup>34</sup> using the ATSAS web interface by applying a P2 symmetry for Suv3, P3 symmetry for PNPase, and P1 symmetry for Suv3 $\Delta$ C and Suv3-PNPase complex. Additionally, electron density maps from SAXS data was generated with DENSS,<sup>33</sup> with a total of 20 multiple reconstructions that were averaged and aligned with a two-fold symmetry for Suv3, three-fold symmetry for PNPase, and no symmetry for PNPase-Suv3 complex to produce the final electron density map.

Structural analysis, visualization and figure preparation of all SAXS models were performed using UCSF Chimera.<sup>43</sup> The crystal structure of the apo-form of Suv3 monomer (PDB entry: 7W1R) was fitted into the Suv3 $\Delta$ C envelope while two monomeric units of apo-form Suv3 was fitted into Suv3 dimer envelope using UCSF Chimera.

#### 4.7 | Exoribonuclease activity of PNPase

For RNA degradation assays, 10 nM of Suv3-PNPase protein complex was incubated with 100 nM of 5'-end FAM-labeled dsRNA and 5 μM of competitive unlabeled RNA oligonucleotide at 37°C in the reaction buffer containing 20 mM Tris-HCl (pH 7.5), 50 mM NaCl, 5 mM NaH<sub>2</sub>PO<sub>4</sub>, 1 mM DTT, 1 mM MgCl<sub>2</sub>, and 5 mM ATP. Reactions were terminated by adding equal amount of 2X Urea loading dye (BIO-RAD) at indicated time points (0–60 min) and heating at 95°C for 3 min. Samples were loaded and separated by 20% polyacrylamide gel containing 7 M urea, visualized using a Typhoon FLA 9000 scanner (GE Healthcare), and quantified in Image J software. The RNA substrate used in the degradation assays were purchased from MdBio Inc. with a sequence of:

5'-FAM-GCGUCUGCAGCGUAUGCCACCACACCAGGA GAGGAGAGGAG-3' and 5'-GGUGUGGUGGCAUACGUG CAGACGC-3'. These two RNA strands were annealed to generate a 20-basepair RNA duplex with a 20-nt 3' overhang.

#### ACKNOWLEDGMENTS

The authors thank the staff members of SAXS beamline TPS-13A1, in the National Synchrotron Radiation Research Center, Hsin-Chu, Taiwan and the crystal diffraction beamline BL44XU in SPring-8, Harima, Japan. We also acknowledge the Biophysics Core of the Institute of Molecular Biology for work on the MALS and fluorescence-based assays. This work was supported by a research grant from Academia Sinica, Taiwan (AS-IA-110-L02 to H.S.Y.).

#### AUTHOR CONTRIBUTIONS

**Monika Jain:** Data curation (lead); formal analysis (lead); investigation (lead); methodology (lead); writing – original draft (equal). **Bagher Golzarroshan:** Data curation (equal); formal analysis (equal). **Chia-Liang Lin:** Data curation (equal); formal analysis (equal). **Sashank Agrawal:** Formal analysis (equal); visualization (equal). **Wei-Hsuan Tang:** Formal analysis (equal). **Chiu-Ju Wu:** Formal analysis (equal). **Hanna S. S. Yuan:** Conceptualization (lead); resources (lead); supervision (lead); validation (lead); writing – review and editing (lead).

## ORCID

Hanna S. Yuan  <https://orcid.org/0000-0001-9671-6967>

## REFERENCES

1. Butow RA, Zhu H, Perlman P, Conrad-Webb H. The role of a conserved dodecamer sequence in yeast mitochondrial gene expression. *Genome*. 1989;31:757–760.
2. Dmochowska A, Kalita K, Krawczyk M, et al. A human putative Suv3-like RNA helicase is conserved between *Rhodobacter* and all eukaryotes. *Acta Biochim Pol*. 1999;46:155–162.
3. Byrd AK, Raney KD. Superfamily 2 helicases. *Front Biosci (Landmark Ed)*. 2012;17:2070–2088.
4. Fairman-Williams ME, Guenther UP, Jankowsky E. SF1 and SF2 helicases: Family matters. *Curr Opin Struct Biol*. 2010;20:313–324.
5. Johnson SJ, Jackson RN. Ski2-like RNA helicase structures: Common themes and complex assemblies. *RNA Biol*. 2013;10:33–43.
6. Jedrzejczak R, Wang J, Dauter M, Szczesny RJ, Stepień PP, Dauter Z. Human Suv3 protein reveals unique features among SF2 helicases. *Acta Crystallogr D Biol Crystallogr*. 2011;67:988–996.
7. Ding L, Liu Y. Borrowing nuclear DNA helicases to protect mitochondrial DNA. *Int J Mol Sci*. 2015;16:10870–10887.
8. Khidr L, Wu G, Davila A, Procaccio V, Wallace D, Lee WH. Role of SUV3 helicase in maintaining mitochondrial homeostasis in human cells. *J Biol Chem*. 2008;283:27064–27073.
9. Shu Z, Vijayakumar S, Chen CF, Chen PL, Lee WH. Purified human SUV3p exhibits multiple-substrate unwinding activity upon conformational change. *Biochemistry*. 2004;43:4781–4790.
10. Khemici V, Linder P. RNA helicases in RNA decay. *Biochem Soc Trans*. 2018;46:163–172.
11. Wang DD, Shu Z, Lieser SA, Chen PL, Lee WH. Human mitochondrial SUV3 and polynucleotide phosphorylase form a 330-kDa heteropentamer to cooperatively degrade double-stranded RNA with a 3'-to-5' directionality. *J Biol Chem*. 2009;284:20812–20821.
12. Borowski LS, Dziembowski A, Hejnowicz MS, Stepień PP, Szczesny RJ. Human mitochondrial RNA decay mediated by PNPase-hSuv3 complex takes place in distinct foci. *Nucleic Acids Res*. 2013;41:1223–1240.
13. Dziembowski A, Piwowarski J, Hoser R, et al. The yeast mitochondrial degradosome. Its composition, interplay between RNA helicase and RNase activities and the role in mitochondrial RNA metabolism. *J Biol Chem*. 2003;278:1603–1611.
14. Razew M, Warkocki Z, Taube M, et al. Structural analysis of mtEXO mitochondrial RNA degradosome reveals tight coupling of nuclease and helicase components. *Nat Commun*. 2018;9:97.
15. Szczesny RJ, Borowski LS, Brzezniak LK, et al. Human mitochondrial RNA turnover caught in flagranti: Involvement of hSuv3p helicase in RNA surveillance. *Nucleic Acids Res*. 2010;38:279–298.
16. Guo XE, Chen CF, Wang DD, et al. Uncoupling the roles of the SUV3 helicase in maintenance of mitochondrial genome stability and RNA degradation. *J Biol Chem*. 2011;286:38783–38794.
17. Clemente P, Pajak A, Laine I, et al. SUV3 helicase is required for correct processing of mitochondrial transcripts. *Nucleic Acids Res*. 2015;43:7398–7413.
18. Pereira M, Mason P, Szczesny RJ, et al. Interaction of human SUV3 RNA/DNA helicase with BLM helicase; loss of the SUV3 gene results in mouse embryonic lethality. *Mech Aging Dev*. 2007;128:609–617.
19. Chen PL, Chen CF, Chen Y, et al. Mitochondrial genome instability resulting from SUV3 haploinsufficiency leads to tumorigenesis and shortened lifespan. *Oncogene*. 2013;32:1193–1201.
20. Pajak A, Laine I, Clemente P, et al. Defects of mitochondrial RNA turnover lead to the accumulation of double-stranded RNA in vivo. *PLoS Genet*. 2019;15:e1008240.
21. Dhir A, Dhir S, Borowski LS, et al. Mitochondrial double-stranded RNA triggers antiviral signalling in humans. *Nature*. 2018;560:238–242.
22. Silva S, Camino LP, Aguilera A. Human mitochondrial degradosome prevents harmful mitochondrial R loops and mitochondrial genome instability. *Proc Natl Acad Sci U S A*. 2018;115:11024–11029.
23. Szczesny RJ, Obriot H, Paczkowska A, et al. Down-regulation of human RNA/DNA helicase SUV3 induces apoptosis by a caspase- and AIF-dependent pathway. *Biol Cell*. 2007;99:323–332.
24. Veno ST, Kulikowicz T, Pestana C, Stepień PP, Stevnsner T, Bohr VA. The human Suv3 helicase interacts with replication protein A and flap endonuclease 1 in the nucleus. *Biochem J*. 2011;440:293–300.
25. Lin PH, Lin-Chao S. RhlB helicase rather than enolase is the beta-subunit of the *Escherichia coli* polynucleotide phosphorylase (PNPase)-exoribonucleolytic complex. *Proc Natl Acad Sci U S A*. 2005;102:16590–16595.
26. Lehnik-Habrink M, Pfortner H, Rempeters L, Pietack N, Herzberg C, Stulke J. The RNA degradosome in *Bacillus subtilis*: Identification of CshA as the major RNA helicase in the multiprotein complex. *Mol Microbiol*. 2010;77:958–971.
27. Golzarroshan B, Jain M, Yuan HS. RNA-binding proteins in bacterial and mitochondrial RNA decay. In: Joseph J, editor. *Encyclopedia of biological chemistry*. Volume 3. 3rd ed., 2021; p. 517–526. Oxford: Elsevier.
28. Bruce HA, Du D, Matak-Vinkovic D, Bandyra KJ, et al. Analysis of the natively unstructured RNA/protein-recognition core in the *Escherichia coli* RNA degradosome and its interactions with regulatory RNA/Hfq complexes. *Nucleic Acids Res*. 2018;46:387–402.
29. Huen J, Lin CL, Golzarroshan B, Yi WL, Yang WZ, Yuan HS. Structural insights into a unique dimeric DEAD-box helicase CshA that promotes RNA decay. *Structure*. 2017;25:469–481.
30. Marcaida MJ, Kauzlaric A, Duperrex A, et al. The human RNA helicase DDX21 presents a dimerization interface necessary for helicase activity. *iScience*. 2020;23:101811.
31. Combet C, Blanchet C, Geourjon C, Deléage G. NPS@: Network protein sequence analysis. *Trends Biochem Sci*. 2000;25:147–150.
32. Jankowsky E. RNA helicases at work: Binding and rearranging. *Trends Biochem Sci*. 2011;36:19–29.
33. Grant TD. Ab initio electron density determination directly from solution scattering data. *Nat Methods*. 2018;15:191–193.
34. Svergun DI, Petoukhov MV, Koch MH. Determination of domain structure of proteins from X-ray solution scattering. *Biophys J*. 2001;80:2946–2953.
35. Svergun DI. Restoring low resolution structure of biological macromolecules from solution scattering using simulated annealing. *Biophys J*. 1999;76:2879–2886.



36. Lin CL, Wang YT, Yang WZ, Hsiao YY, Yuan HS. Crystal structure of human polynucleotide phosphorylase: Insights into its domain function in RNA binding and degradation. *Nucleic Acids Res.* 2012;40:4146–4157.
37. Hardwick SW, Gubbey T, Hug I, Jenal U, Luisi BF. Crystal structure of *Caulobacter crescentus* polynucleotide phosphorylase reveals a mechanism of RNA substrate channelling and RNA degradosome assembly. *Open Biol.* 2012;2:120028.
38. Gwynn EJ, Smith AJ, Guy CP, Savery NJ, McGlynn P, Dillingham MS. The conserved C-terminus of the PcrA/UvrD helicase interacts directly with RNA polymerase. *PLoS One.* 2013;8:e78141.
39. Fazala FM, Kosloverb DJ, Luisi BF, Blocka SM. Direct observation of processive exonuclease motion using optical tweezers. *Proc Natl Acad Sci U S A.* 2015;112:15101–15106.
40. Hopkins JB, Gillilan RE, Skou S. BioXTAS RAW: Improvements to a free open-source program for small-angle X-ray scattering data reduction and analysis. *J Appl Cryst.* 2017;50:1545–1553.
41. Manalastas-Cantos K, Konarev PV, Hajizadeh NR, et al. ATSAS 3.0: Expanded functionality and new tools for small-angle scattering data analysis. *J Appl Cryst.* 2021;54:343–355.
42. Svergun D. Determination of the regularization parameter in indirect-transform methods using perceptual criteria. *J Appl Cryst.* 1992;25:495–503.
43. Pettersen EF, Goddard TD, Huang CC, et al. UCSF chimera--A visualization system for exploratory research and analysis. *J Comput Chem.* 2004;25, 1605–1612.

## SUPPORTING INFORMATION

Additional supporting information may be found in the online version of the article at the publisher's website.

**How to cite this article:** Jain M, Golzarroshan B, Lin C-L, Agrawal S, Tang W-H, Wu C-J, et al. Dimeric assembly of human Suv3 helicase promotes its RNA unwinding function in mitochondrial RNA degradosome for RNA decay. *Protein Science.* 2022;31(5):e4312. <https://doi.org/10.1002/pro.4312>